

## Article

# A Dual Reactor for Isothermal Thermochemical Cycles of H<sub>2</sub>O/CO<sub>2</sub> Co-Splitting Using La<sub>0.3</sub>Sr<sub>0.7</sub>Co<sub>0.7</sub>Fe<sub>0.3</sub>O<sub>3</sub> as an Oxygen Carrier

Tatiya Khamhangdatepon <sup>1</sup>, Thana Sornchamni <sup>2</sup>, Nuchanart Siri-Nguan <sup>2</sup>, Navadol Laosiripojana <sup>3</sup> and Unalome Wetwatana Hartley <sup>1,3,\*</sup> 

<sup>1</sup> Mechanical and Process Engineering Department, Sirindhorn International Institute of Technology, King Mongkut's University of Technology North Bangkok, Bangkok 10800, Thailand; khamhangdatepon.tatiya@gmail.com

<sup>2</sup> PTT Research and Technology Institute, PTT Public Company Limited, Bangkok 10900, Thailand; thana.s@pttplc.com (T.S.); nuchanart.s@pttplc.com (N.S.-N.)

<sup>3</sup> The Joint Graduate School of Energy and Environment, King Mongkut's University of Technology Thonburi, Bangkok 10140, Thailand; navadol@jgsee.kmutt.ac.th

\* Correspondence: unalome.w.cpe@tggs-bangkok.org



**Citation:** Khamhangdatepon, T.; Sornchamni, T.; Siri-Nguan, N.; Laosiripojana, N.; Hartley, U.W. A Dual Reactor for Isothermal Thermochemical Cycles of H<sub>2</sub>O/CO<sub>2</sub> Co-Splitting Using La<sub>0.3</sub>Sr<sub>0.7</sub>Co<sub>0.7</sub>Fe<sub>0.3</sub>O<sub>3</sub> as an Oxygen Carrier. *Processes* **2021**, *9*, 1018. <https://doi.org/10.3390/pr9061018>

Academic Editors: Gianvito Vilé and Jiaxu Liu

Received: 25 March 2021

Accepted: 4 June 2021

Published: 9 June 2021

**Publisher's Note:** MDPI stays neutral with regard to jurisdictional claims in published maps and institutional affiliations.



**Copyright:** © 2021 by the authors. Licensee MDPI, Basel, Switzerland. This article is an open access article distributed under the terms and conditions of the Creative Commons Attribution (CC BY) license (<https://creativecommons.org/licenses/by/4.0/>).

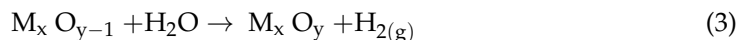
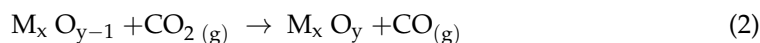
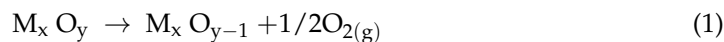
**Abstract:** Catalytic performance of La<sub>0.3</sub>Sr<sub>0.7</sub>Co<sub>0.7</sub>Fe<sub>0.3</sub>O<sub>3</sub> (LSCF3773 or LSCF) catalyst for syngas production via two step thermochemical cycles of H<sub>2</sub>O and CO<sub>2</sub> co-splitting was investigated. Oxygen storage capacity (OSC) was found to depend on reduction temperature, rather than the oxidation temperature. The highest oxygen vacancy ( $\Delta\delta$ ) was achieved when the reduction and oxidation temperature were both fixed at 900 °C with the feed ratio (H<sub>2</sub>O to CO<sub>2</sub>) of 3 to 1, with an increasing amount of CO<sub>2</sub> in the feed mixture. CO productivity reached its plateau at high ratios of H<sub>2</sub>O to CO<sub>2</sub> (1:1, 1:2, and 1:2.5), while the total productivities were reduced with the same ratios. This indicated the existence of a CO<sub>2</sub> blockage, which was the result of either high  $E_a$  of CO<sub>2</sub> dissociation or high  $E_a$  of CO desorption, resulting in the loss in active species. From the results, it can be concluded that H<sub>2</sub>O and CO<sub>2</sub> splitting reactions were competitive reactions.  $E_a$  of H<sub>2</sub>O and CO<sub>2</sub> splitting was estimated at 31.01 kJ/mol and 48.05 kJ/mol, respectively, which agreed with the results obtained from the experimentation of the effect of the oxidation temperature. A dual-reactors system was applied to provide a continuous product stream, where the operation mode was switched between the reduction and oxidation step. The isothermal thermochemical cycles process, where the reduction and oxidation were performed at the same temperature, was also carried out in order to increase the overall efficiency of the process. The optimal time for the reduction and oxidation step was found to be 30 min for each step, giving total productivity of the syngas mixture at 28,000 μmol/g, approximately.

**Keywords:** perovskite; La<sub>0.3</sub>Sr<sub>0.7</sub>Co<sub>0.7</sub>Fe<sub>0.3</sub>O<sub>3</sub>; LSCF; CO<sub>2</sub> utilization; continuous two-step thermochemical cycles; synthesis gas production

## 1. Introduction

The continuous increase in anthropogenic, atmospheric CO<sub>2</sub> concentrations, and rapid expansion in the widespread use of fossil fuels, such as coal, oil, and natural gas, have resulted in the serious, worldwide greenhouse effect [1,2]. Therefore, the decrease in CO<sub>2</sub> emissions as a most important universal issue has garnered rising interest in recent years. CO<sub>2</sub> as a major greenhouse gas (GHG) considerably contributes to global warming, causing an environmentally dangerous effect. The reprocessing of CO<sub>2</sub> as a carbon source for chemical fuels, using any added energy source, such as solar, geothermal, and even confidently safe nuclear energy, is desirable for the development of a large-scale, cost-effective, sustainable energy system. The “thermochemical cycle” suggests a process for converting heat energy into carbon monoxide and hydrogen, the energy

carriers. In comparison to the direct thermal decomposition of CO<sub>2</sub> and H<sub>2</sub>O at high temperatures, thermochemical methods of CO<sub>2</sub> and H<sub>2</sub>O decomposition are driven at proper lower temperatures by joining high temperature endothermic chemical reactions and low temperature exothermic chemical reactions. As such, they present a smart method for fuel generation at high rates and efficiencies without noble metal catalysts [3], which, via redox chemical reactions, additionally go around the CO–H<sub>2</sub>–O<sub>2</sub> separation problem [4]. Two step thermochemical cycles support for metal oxide redox pairs (mostly La/La<sub>2</sub>O<sub>3</sub>, Sr/SrO<sub>2</sub>, Co/CoO<sub>3</sub> Zn/ZnO, Ce<sub>2</sub>O<sub>3</sub>/CeO<sub>2</sub>, FeO/Fe<sub>3</sub>O<sub>4</sub> and SnO/SnO<sub>2</sub>), to date, have mostly been reported, which are determined by high temperature process heat [4–15]. The major challenges are the requirement of rapid reduction in gaseous products to avoid their recombination [4] and the entire conversion of metal to metal-oxide to execute fast carbon monoxide and hydrogen production rates [10]. To overcome those challenges, multi metal/metal oxides composite as catalysts are very suitable for thermochemical two-step thermochemical cycles of H<sub>2</sub>O/CO<sub>2</sub> co-splitting. Two-step thermochemical metal/metal oxide cycles are explained by the subsequent chemical steps. The net effect of reactions (Equations (1)–(3)) is the preferred splitting of water and carbon dioxide by way of using the metal oxide as a catalyst.



Among all metal/metal oxides, lanthanum (La)-cobalt (Co)-based catalysts are shown great attention and have been examined due to their high reduction extent. However, both their re-oxidation coverage and generation stability are low, making them unfit for thermochemical applications, which have numerous successive redox cycles [16]. An approach for incorporating lanthanum–cobalt with Ca<sup>2+</sup> or Sr<sup>2+</sup> in the A-site or with Cr and Fe in the B-site was reported, but in all composites, the fuel generation decreased over cycles [15–21]. Further, researchers are focused on La–Co with multi metal/metal oxides. Hence, La–Co doped with Sr and Fe (A and B site substitution) has been widely reported for assessing its thermochemical performance. Moreover, the thermal dissociation of Fe<sub>3</sub>O<sub>4</sub> to FeO has also been experimentally investigated at temperatures between 1700 and 2000 °C and pressures of 0.1–1 bar in with inert and air atmospheres [22,23]. The second step of the cycle is a low-temperature, exothermic reaction, where the reduced metal reacts with a mixture of H<sub>2</sub>O and CO<sub>2</sub> to generate H<sub>2</sub> and CO (syngas), which is readily used, while its ratio can be tailor-made. The Sr<sup>2+</sup> cation in the A-site leads to an increase in the Fe oxidation state for electronic neutrality, which allows increasing the reduction extent. One of the challenges is that while the operating temperature is switching between the endothermic reduction reaction to the exothermic oxidation reaction, the overall efficiency of the process will be lost, as the system requires extra time to reach the desired temperature. This work, therefore, studied isothermal thermochemical cycles where the reduction and oxidation step were handled at the same temperature in order to reduce the thermal stress within the system by eliminating the time loss due to reaching different temperatures of reduction and oxidation, thus increasing the overall efficiency. To enhance the system to produce a continuous product stream, a dual reactor was applied, aiming to continuously double the productivity.

## 2. Methodology

### 2.1. Catalyst Preparation and Characterization

LSCF3773 was synthesized, using the ethylenediaminetetraacetic acid (EDTA)-citrate complexing method [24]. The molar ratio of total citric acid to metal ions to EDTA was 3:2:2. A homogenous EDTA-NH<sub>3</sub>·H<sub>2</sub>O solution was prepared by slowly adding 0.05 mol of EDTA to 100 mL of ammonium (NH<sub>3</sub>·H<sub>2</sub>O) solution (1 M) while stirred at 500 rpm at a temperature of 80 °C. The nitrate salts of the metals, i.e., Sr(NO<sub>3</sub>)<sub>2</sub> ( $\geq 98.00\%$  HiMedia,

Mumbai, India),  $\text{La}(\text{NO}_3)_3 \cdot 6\text{H}_2\text{O}$  ( $\geq 99.00\%$ , HiMedia, Mumbai, India),  $\text{Co}(\text{NO}_3)_2 \cdot 6\text{H}_2\text{O}$  ( $\geq 99.00\%$ , Carlo Erba Reagents, Val-de-Reuil, France) and  $\text{Fe}(\text{NO}_3)_3 \cdot 9\text{H}_2\text{O}$  ( $\geq 99.00\%$ , Ajax Finechem, Victoria, Australia), were slowly added to the  $\text{EDTA-NH}_3 \cdot \text{H}_2\text{O}$ . The solution was stirred continuously to ensure its homogeneous state. A total of 0.07 mols of citric acid was added to the solution, while pH was maintained at 4.9 to 6.9 by the addition of an ammonium solution. A dark purple gel was formed after the well-mixed solution was stirred and heated at  $120^\circ\text{C}$  for 5 h. The gel was placed in a vacuum oven at  $180^\circ\text{C}$  for 48 h until a dark-brown dried foam was produced. The dried foam was ground to powder before being calcined at  $500^\circ\text{C}$  for 5 h in order to eliminate an excess of polymeric substances, then at  $1100^\circ\text{C}$  for 10 h to obtain the perovskite phase structure. The resulting fine LSCF3773 powder was pelletized, using a hydraulic press. The pelletized LSCF3773 was further ground and sieved to a  $180\text{--}212\text{ }\mu\text{m}$  size range.

The material's crystallinity and purity were characterized using X-ray diffraction (XRD, Bruker AXS, Diffractometer D8, Billerica, MA, USA) equipment, using  $\text{CuK}-\alpha$  radiation with  $\lambda = 1.5418\text{ \AA}$  as a radiation source at 40 kV and 30 mA with a scanning speed of  $0.02^\circ/\text{s}$  in the range of  $10^\circ < 2\theta < 80^\circ$ . The transient characterization, i.e., temperature programmed reduction (TPR) and temperature programmed desorption (TPD) are described in the later section, as they were experimentally tested in an in-house reactor.

## 2.2. Experimental Procedure

### 2.2.1. Reactor Set-Up

Thermochemical cycles of  $\text{H}_2\text{O}/\text{CO}_2$  splitting were carried out in a dual lab-scale packed-bed reactor system as shown in Figure 1. Reactors Nos. 1 and 2 were set up for continuous two-step thermochemical cycles to operate alternately during reduction and oxidation steps. The lab-prepared LSCF3773 was packed in the center of quartz tubular reactors (i.d. = 13 mm.), which was supported vertically in an electrical tubular furnace ( $1100^\circ\text{C}$  max temperature, 20 cm long, Inconel, Suan-luang Engineering, Bangkok, Thailand). Quartz wool was used to immobilize the packed LSCF3773. K-type thermocouple was inserted at the center of the heating-zone nearest to the catalyst's bed. Gaseous reagents  $\text{CO}_2$  (99.9%, Bangkok Industrial Gas (BIG), Bangkok, Thailand), Ar (99.95%, BIG) and 10%  $\text{H}_2$  in Ar (BIG) were introduced into the system, using mass flow controllers (MFC) (New Flow-TLFC-00-A-1-W-2, Golden Mountain Enterprise, Kaohsiung 806, Taiwan). The steam generators were made in-house by connecting a peristaltic pump (model: BT100M, Baoding Chuang Rui Precision Pump, Hebei, China) with an evaporator (Suan-luang Engineering, Bangkok, Thailand). Deionized water was supplied to the peristaltic pump at a flow rate of 0.07 mL/min in every testing condition. The steam generator outlet was connected to the Ar gas pipeline to help convey saturated steam to the packed bed reactors. The steam pipeline was insulated by wrapping with heating tape with its temperature maintained at  $130^\circ\text{C}$  to avoid condensation. The reactor effluent was passed through a condenser unit and filter to ensure a dried-gaseous stream before entering the on-line mass spectrometers (OMNI Star, Pfeiffer vacuum, Aßlar, Germany).

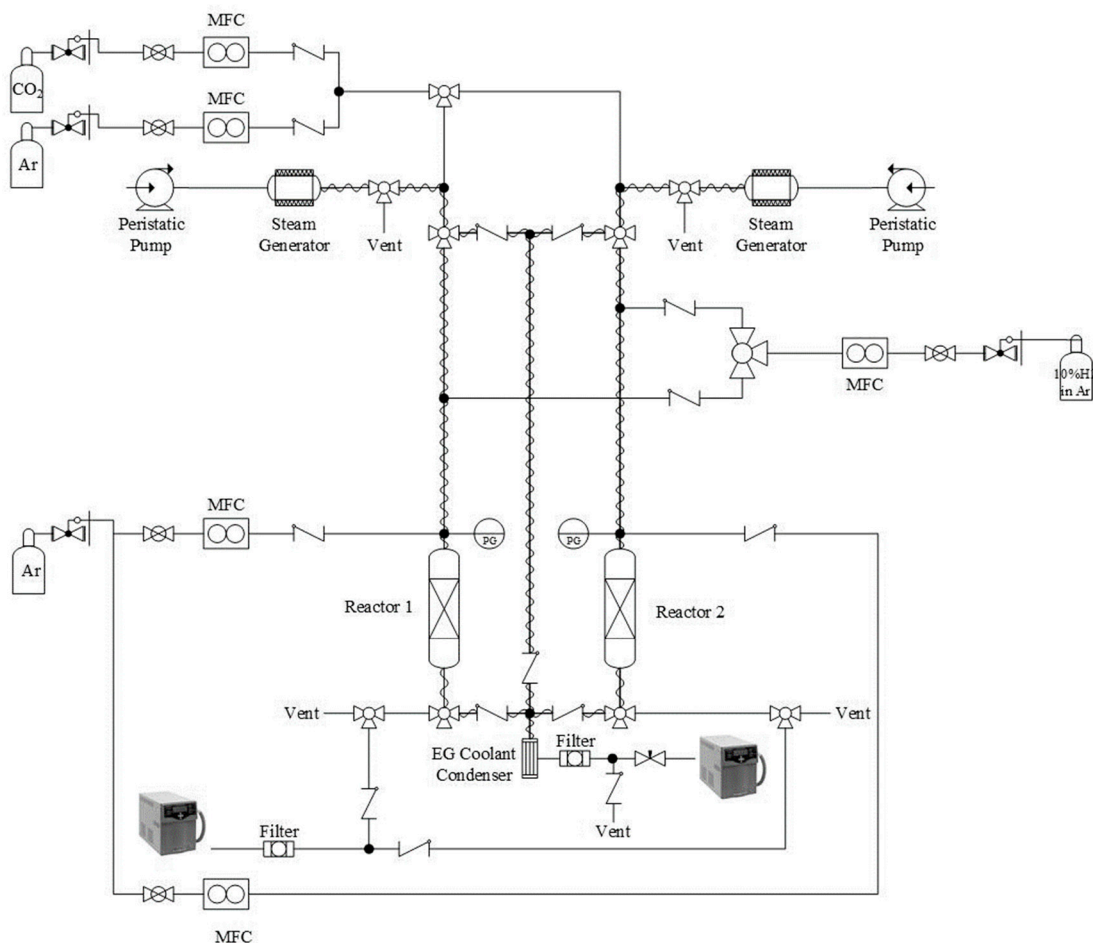


**Figure 1.** A dual reactor for continuous 2-step thermochemical cycles of  $\text{H}_2\text{O}$  and  $\text{CO}_2$  co-splitting, equipped with 2 on-line mass spectrometers.

### 2.2.2. Single Reactor Experiments

The reaction was performed in a single packed bed reactor under different sets of reduction/oxidation temperatures, varying from 500, 700 and 900  $^{\circ}\text{C}$ . A total of 0.5 g of LSCF3773 powder was used for these experimentations. For the reduction step, 100  $\text{mL}\cdot\text{min}^{-1}$  of 10 %  $\text{H}_2$  in Ar was fed through the packed bed reactor for 30 min under the set reduction temperature shown in Table 1. During the oxidation step, gaseous  $\text{H}_2\text{O}/\text{CO}_2$  with specific ratios was introduced into the reactor while the total flow rate of each test was also kept constant as tabulated in Table 1. Before switching the reactor conditions to be between reduction and oxidation, 300  $\text{mL}\cdot\text{min}^{-1}$  of pure Ar was flowed through the system for 30 min to remove remaining gaseous compounds or any physisorptions. The reduction and oxidation step of each condition was cycled for 5 cycles. Production yields of  $\text{H}_2$  and  $\text{CO}_2$  were averaged using information received via those 5 cycles.

**Table 1.** Experiment conditions.

Condition No.	H <sub>2</sub> O/CO <sub>2</sub> Molar Ratio	H <sub>2</sub> O Molar Flow Rate (mmol/min)	CO <sub>2</sub> Molar Flow Rate (mmol/min)	Total Flow Rate (mL/min)	Reduction Temperature (°C)	Oxidation Temperature (°C)
1	1 to 1	3.89	3.89	200	500	500
2	1 to 1	3.89	3.89	200	700	700
3	1 to 1	3.89	3.89	200	900	900
4	1 to 1	3.89	3.89	200	500	900
5	1 to 1	3.89	3.89	200	700	900
6	1 to 1	3.89	3.89	200	900	500
7	1 to 1	3.89	3.89	200	900	700
8	3 to 1	3.89	1.30	200	900	900
9	1.5 to 1	3.89	2.59	200	900	900
10	1 to 2	3.89	7.79	200	900	900
11	1 to 2.5	3.89	9.72	250	900	900

### 2.2.3. Dual-Reactor System Experiments

The reactivity of LSCF3773 in a dual system was tested for continuous production of H<sub>2</sub> and CO as shown in Figure 1. The operation mode of both reactors was switched between reduction and oxidation, as illustrated in Figure 2, in order to produce a continuous stream of the product. A total of 0.5 g of LSCF3773 was packed in both reactors. Prior to the experiment, the packed LSCF3773 was reduced beforehand with 10.0% H<sub>2</sub> in Ar for 15 min at a temperature of 900 °C. The procedure is also considered a reduction step as well as a pre-treatment step. The system was purged by 300 mL·min<sup>-1</sup> of Ar for 15 min to remove any possible physisorption/unwanted residuals. During the oxidation step (first production step), a mixture of H<sub>2</sub>O:CO<sub>2</sub> (1:1.25) was introduced into the interest reactor. Both reactors took turns to carry out the reduction and oxidation step in a cycling manner. The reactors were operated alternately as a looping sequence for 20 cycles. Together, the 2 reactors were able to produce a continuous stream of the product, which was a mixture of H<sub>2</sub> and CO. Two mass spectrometers were connected on-line to each reactor to analyze the outlet gaseous stream.

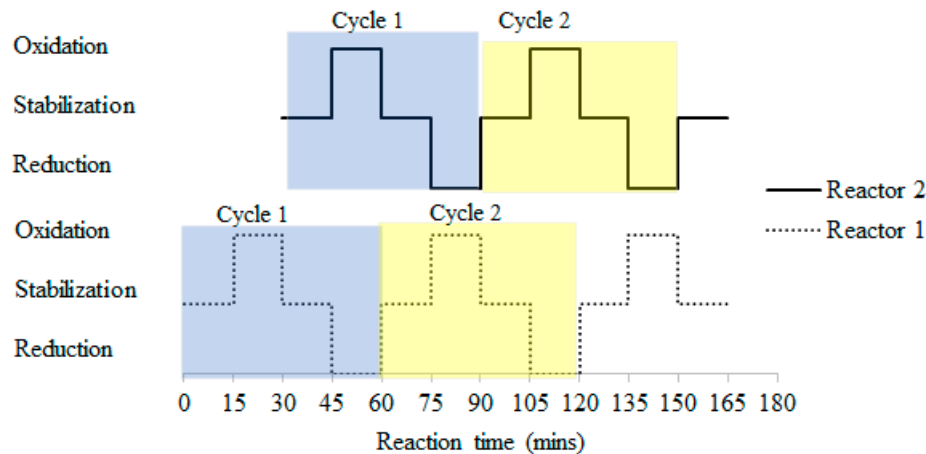


**Figure 2.** The operating mode, cycling time and procedure for the dual reactor system for experimenting on the two-step thermochemical cycles.

#### 2.2.4. Solid Conversion and Reactive Gases Conversion

Total solids conversion  $X(t)$  as a function of time in Equation (4) is denoted by the ratio of total amount of  $H_2$  and  $CO$  produced at any time ( $t$ ) to the initial available amount of oxygen vacancies in the LSCF sample as follows:

$$X(t) = \frac{n_{o\ reacted}}{n_{o\ available}} = \frac{n_{MO_x}(t)}{n_{MO_{x-\delta,in}}} = \frac{\int_0^t (F_{H_2} + F_{CO}) dt}{n_{MO_{x-\delta,in}}} \quad (4)$$

$F_{H_2}$  and  $F_{CO}$  denote the accumulative amount of  $H_2$  and  $CO$  produced, estimated by integration of the production rate profile in Equations (5) and (6),  $n_{MO_{x-\delta,in}}$  is the number of oxygen vacancies provided by  $H_2$ -TPR result, and  $t$  is the reaction time (min).

$$F_{H_2}(t) = y_{H_2}(t) \cdot v_o \quad (5)$$

$$F_{CO}(t) = y_{CO}(t) \cdot v_o \quad (6)$$

where  $y_{H_2}(t)$  and  $y_{CO}(t)$  are mole fractions of the outlet of  $H_2$  and  $CO$  at time ( $t$ ), while  $v_o$  represents the total outlet molar gas flow rate (mol/min).

Reactive gas conversions can be represented by the ratio of accumulated molar amounts of product gas to the inlet molar flow rates of reactive gas and total reaction time according to Equations (7) and (8).

$$H_2O\ conversion = \frac{n_{H_2}}{(F_{H_2O,in} \cdot t)} \quad (7)$$

$$CO_2\ conversion = \frac{n_{CO}}{(F_{CO_2,in} \cdot t)} \quad (8)$$

where  $n_{H_2}$  and  $n_{CO}$  are the accumulated molar amounts of  $H_2$  or  $CO$  (mol),  $F_{H_2O,in}$  and  $F_{CO_2,in}$  represent the inlet molar flowrates of  $H_2O$  or  $CO_2$  (mol/min), and  $t$  is the total reaction time (min).

#### 2.2.5. Gas-Solid Kinetics Analysis

Reaction rates can be generally described as Equation (9):

$$\frac{dX}{dt} = k \cdot f(X) \quad (9)$$

where  $f(X)$  is a solid conversion selected from solid-state kinetic models, assuming formation of new product occurs at the reactive species/points in the lattice of the solid material. The Avrami model is illustrated as shown in Equation (10) below:

$$[-\ln(1 - X)]^{\frac{1}{n}} = kt \quad (10)$$

where  $X$  is the solid conversion.

The overall rate of reaction concerning temperature dependency was, therefore, determined by associating the above equations with the Arrhenius Law, as shown in Equation (11):

$$k(T) = k_0 \cdot e^{-\frac{E_a}{RT}} \quad (11)$$

Kinetic parameters, i.e., activation energy ( $E_a$ ) and the pre-exponential factor ( $k_0$ ) were then graphically estimated. The experimental data were compared to the kinetics model, using the non-linear regression method.

### 3. Result and Discussion

#### 3.1. Reactivity Study

The catalytic reactivity of LSCF3773 toward the two-step thermochemical cycles of  $\text{H}_2\text{O}/\text{CO}_2$  co-splitting was studied in a single packed bed reactor. Reverse water gas shift (RWGS) and water gas shift (WGS) were considered non-existent, as the products (either  $\text{H}_2$  or  $\text{CO}$ ) were not in contact with the reactants ( $\text{H}_2\text{O}$  or  $\text{CO}_2$ ) during this kind of operation. The results, where different reduction and oxidation temperatures were constant and varied, were selected as shown in Figure 3, whereas the effect of the molar feed ratio is illustrated in Figure 4. From Figure 3, it can be seen that all the graphs were steeply increasing during the first 5 min, indicating that the reaction occurred under the interfacial mass transfer regime. After 5 to 10 min passed, a diffusion control-based reaction took place where the solid conversion slowed down while reaching its equilibrium concentration after 25 min, approximately, for all the cases.

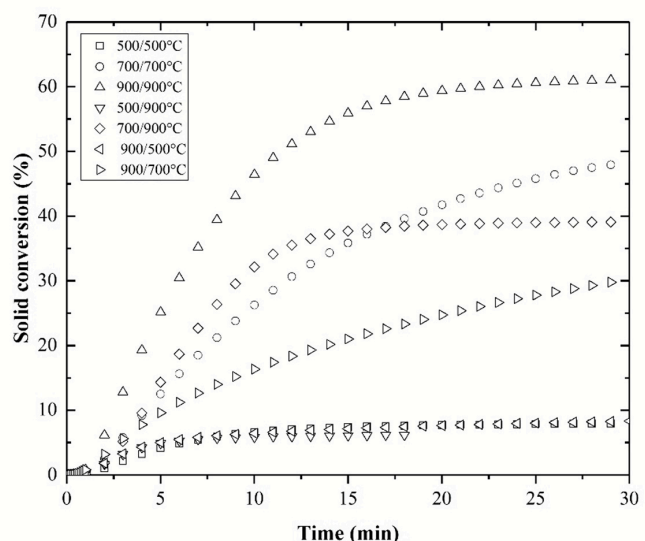


**Figure 3.** Solid conversion of LSCF3773 (%) with feed ratio of  $\text{H}_2\text{O}$  to  $\text{CO}_2$  was 1 to 1, and  $T_{\text{red}}/T_{\text{ox}}$  were paired at 500/500, 500/900, 700/700, 700/900, 900/500, 900/700, and 900/900 °C.

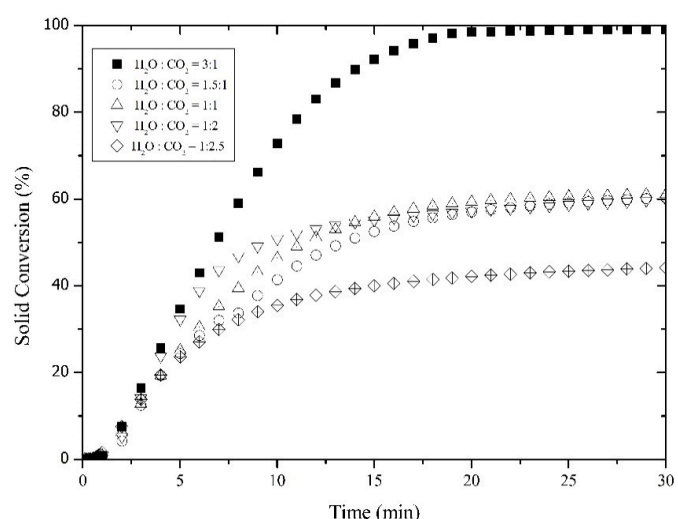


**Figure 4.** Solid conversion of LSCF3773 (%) when  $T_{\text{red}}/T_{\text{ox}}$  was set constant at 900/900 °C, feed ratio of  $\text{H}_2\text{O}$  to  $\text{CO}_2$  was varied at 3 to 1, 1.5 to 1, 1 to 1, 1 to 2, and 1 to 2.5.

The results indicate that at different ranges of reduction temperatures or oxidation temperatures, different initial rates of reaction were measured as shown in Figure 3. Higher reduction temperatures render higher amounts of oxygen vacancies; however, the solid conversion rates are influenced by the temperatures of the exothermic oxidation reaction. It can be noticed that the net conversion of the reaction at 700/900 °C was slightly lower than that at 700/700 °C after reaching equilibrium due to its thermodynamic limitation. At this stage, intrafacial catalysis was proceeded by the redox cycle, involving the solid bulk of the catalyst, becoming the dominant effect with the increased temperature. On the other hand, at low temperatures, the suprafacial catalysis took place on the catalysts' surface at slow rates of reaction. When the molar feed ratio H<sub>2</sub>O/CO<sub>2</sub> was varied under the same conditions with a reaction temperature of 900/900 °C, the solid conversion rate was not influenced by the molar feed ratio at the initial stage. It was noticed that the solid conversion was decreased when the CO<sub>2</sub> content in the feed increased; thus, only a 3 to 1 ratio of H<sub>2</sub>O to CO<sub>2</sub> could provide 100% conversion. This phenomenon was due to the CO<sub>2</sub> blockage caused by CO<sub>2</sub> adsorption in the high CO<sub>2</sub> content feed stream [15].

### 3.2. Reduction Temperature Effect

From Figure 5, it is obvious that the reduction and oxidation temperatures affected the solid conversions. Since the other by-products (i.e., CH<sub>4</sub>) were not detected by the mass spectrometer (MS), the solid conversion thus directly implied syngas productivity. This experimentation showed an effect of the reduction temperature on the productivity of syngas by H<sub>2</sub> and CO, separately, using the MS. The reduction temperature was varied at 500, 700 and 900 °C, while the oxidation temperature was fixed constant at 900 °C. The results are demonstrated in Figure 5. H<sub>2</sub> and CO production increased as the reduction temperature was increased to produce H<sub>2</sub> at 847, 1048 and 1815 μmol/g, respectively. The CO production was measured at 359, 542 and 600 μmol/g, respectively. In general, both H<sub>2</sub> and CO were increased with the reduction temperatures. However, for H<sub>2</sub> production, increasing the reduction temperature from 700 to 900 °C only increased the H<sub>2</sub> production by 10.50%, whereas increasing the reduction temperature from 500 to 700 °C resulted in a larger increase in H<sub>2</sub> of around 51.25%. This indicates that H<sub>2</sub>O splitting occurred on regular cations (Co<sup>+4</sup>, Fe<sup>+4</sup>) and polaron cations (Co<sup>+3</sup>, Fe<sup>+3</sup>), rather than the localized cations (Co<sup>+2</sup>, Fe<sup>+2</sup>) [15]. On the other hand, the CO formation showed the opposite trend, as it increased by only 23.85% when the reduction temperature increased from 500 to 700 °C, and by 73.08% from 700 to 900 °C. Therefore, it can be concluded that while the regular cations (Co<sup>+4</sup>, Fe<sup>+4</sup>) and polaron cations (Co<sup>+3</sup>, Fe<sup>+3</sup>) are served for both H<sub>2</sub>O and CO<sub>2</sub> splitting (with preference on H<sub>2</sub>O splitting), the localized cations (Co<sup>+2</sup> and Fe<sup>+2</sup>) are mostly responsible for the CO<sub>2</sub> splitting. The syngas ratio at the reduction temperature of 500 and 700 °C seems to be feasible with its utilization in the FT process, whereas that at a reduction temperature of 900 °C could be more beneficial for methanol synthesis.

When comparing the H<sub>2</sub> production from this work (Supplementary Materials, H<sub>2</sub>O and CO<sub>2</sub> were co-fed) with the H<sub>2</sub> production from our previous results (feed only pure H<sub>2</sub>O) [15], the H<sub>2</sub> production was estimated at 453, 3109, and 3623 μmol/g·min at reduction temperatures of 500, 700, and 900 °C, respectively. It was obvious that the H<sub>2</sub> production received from the co-reactant feed system was much less than the H<sub>2</sub> production obtained from the pure H<sub>2</sub>O feed system. This indicates that the H<sub>2</sub>O and CO<sub>2</sub> splitting are considered competitive reactions in which H<sub>2</sub>O splitting tends to occur on Co<sup>+4</sup>, Fe<sup>+4</sup> (stage 1 from Figure 4) and Co<sup>+3</sup>, Fe<sup>+3</sup>, while CO<sub>2</sub> splitting prefers to take place on the higher excited stage of Co<sup>+2</sup>, Fe<sup>+2</sup>.

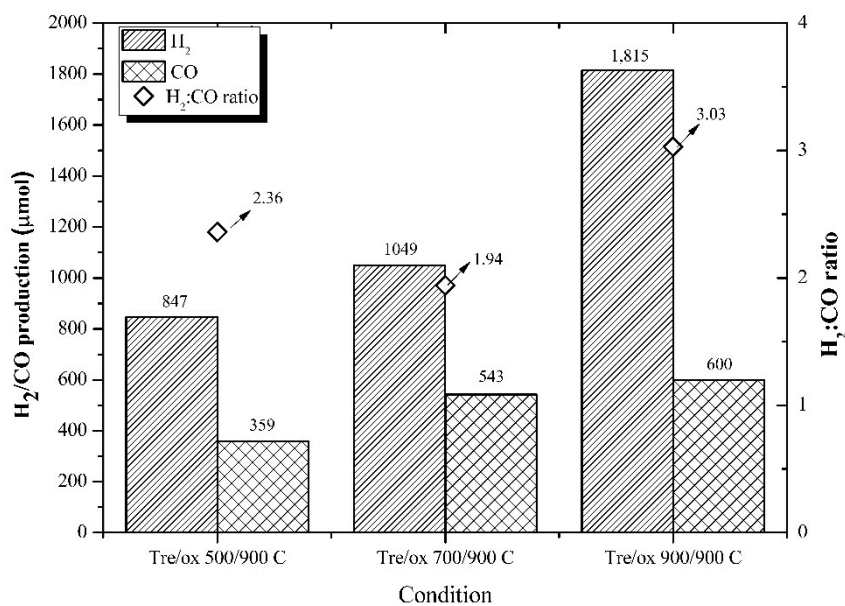


**Figure 5.** Total gas production ( $\mu\text{mol}$ ) and  $\text{H}_2:\text{CO}$  ratio (1) via isothermal  $\text{H}_2\text{O}/\text{CO}_2$  co-splitting over LSCF3773 (feed ratio of  $\text{H}_2\text{O}$  to  $\text{CO}_2$  was 1 to 1,  $T_{\text{red}}/T_{\text{ox}}$  were at 500/900  $^{\circ}\text{C}$ , 700/900  $^{\circ}\text{C}$ , and 900/900  $^{\circ}\text{C}$ ).

### 3.3. Oxidation Temperature Effect

Similarly, the influence of oxidation temperature on the productivity of syngas was also determined, as shown in Figure 6. The oxidation temperature was varied at 500, 700, and 900  $^{\circ}\text{C}$ , while the reduction temperature was fixed at the optimal 900  $^{\circ}\text{C}$ .  $\text{H}_2$  productivity was estimated at 261, 1760, and 1815  $\mu\text{mol}$ , while  $\text{CO}_2$  productivity was 57, 174, and 600  $\mu\text{mol}$  when the oxidation temperature was 500, 700, and 900  $^{\circ}\text{C}$ , respectively. For  $\text{H}_2$  production, it can be seen that at temperatures lower than 700  $^{\circ}\text{C}$ , the  $\text{H}_2\text{O}$  splitting reaction was kinetically controlled as the  $\text{H}_2$  productivity was increased (6.7 times from 500 to 700  $^{\circ}\text{C}$ ) with the increasing temperature. However, at temperatures ranging from 700 to 900  $^{\circ}\text{C}$ , an increase in oxidation temperature did not have much influence on  $\text{H}_2$  productivity (only increased around 3% from 700 to 900  $^{\circ}\text{C}$ ), indicating that the  $\text{H}_2\text{O}$  splitting reaction was more thermodynamic-dependent during this temperature range. On the other hand,  $\text{CO}_2$  production seemed to increase proportionally with increasing oxidation temperatures, which was three times from 500 to 700  $^{\circ}\text{C}$ , and another three times from 700 to 900  $^{\circ}\text{C}$ ). It can be concluded that the  $\text{CO}_2$  splitting reaction was kinetically governed throughout the studied oxidation temperature range (500 to 900  $^{\circ}\text{C}$ ). Therefore,  $E_a$  of  $\text{CO}_2$  splitting is expected to be higher than that of  $\text{H}_2\text{O}$  splitting.

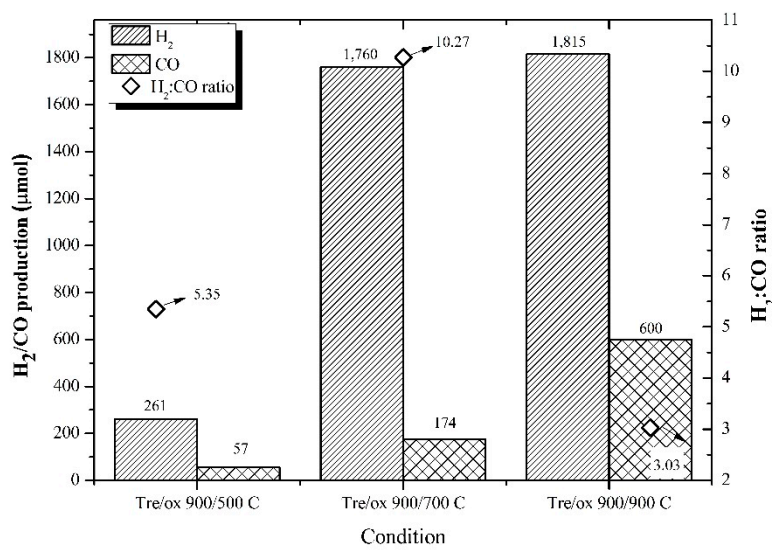


**Figure 6.** Total gas production and  $H_2:CO$  ratio via isothermal  $H_2O/CO_2$  co-splitting over LSCF3773 (feed ratio of  $H_2O/CO_2$  was 1 to 1,  $T_{red}/T_{ox}$  were at 900/500 °C, 900/700 °C, and 900/900 °C).

#### 3.4. Feed Molar Ratio Effect

The ratio of  $H_2O:CO_2$  was varied at 3 to 1, 1.5 to 1, 1 to 1, 1 to 2, and 1 to 2.5, while the reduction and oxidation temperature were both fixed at 900 °C. Figure 7 shows the results summarized as  $H_2$  production decreased with the increasing  $CO_2$ , the total production decreased as the  $CO_2$  ratio was increased, and  $CO$  production slightly increased. This phenomenon confirms that  $H_2O$  splitting and  $CO_2$  splitting are competitive reactions. The  $CO_2$  blockage on the active sites was suggested as the decrease in the total production ( $H_2$  and  $CO$  productivity) and a plateau of  $CO$  production (at higher ratios of  $H_2O/CO_2$  at 1:1, 1:2, and 1:2.5) was evidenced. The results agreed with our previous work in which  $CO_2$  desorption was detected [15]. The high  $E_a$  of  $CO_2$  desorption was determined to be the reason.

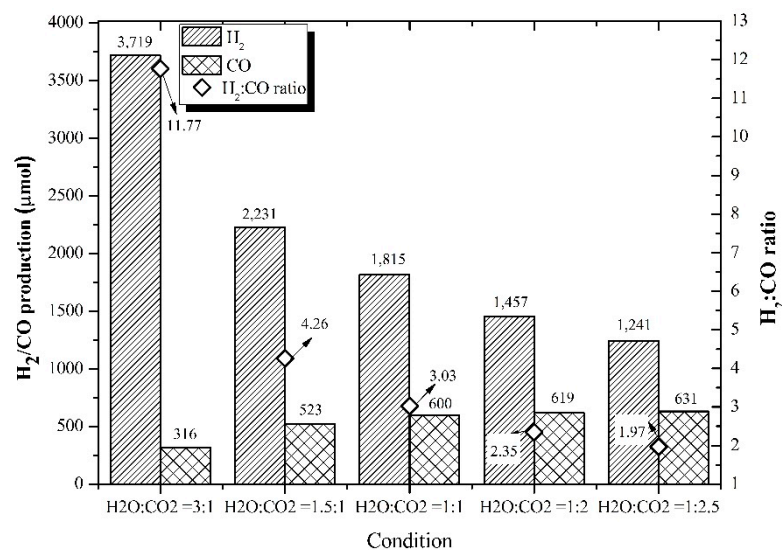


**Figure 7.** Total gas production and  $H_2:CO$  ratio via isothermal  $H_2O/CO_2$  co-splitting over LSCF3773 ( $T_{red}/T_{ox}$  were at 900/900 °C, feed ratio of  $H_2O$  to  $CO_2$  were at 3 to 1, 1.5 to 1, 1 to 1, 1 to 2, and 1 to 2.5 respectively).

From all the previous results, the spent oxygen vacancy can be calculated in terms of  $\Delta\delta$ , the stoichiometric oxygen vacancy in the LSCF3773 ( $\text{La}_{0.3}\text{Sr}_{0.7}\text{Cr}_{0.7}\text{Fe}_{0.3}\text{O}_{3-\delta}$ ), using the following equation:

$$|\Delta\delta(t)| = \frac{n_0(t)}{n_{LSCF}} \quad (12)$$

where:

$$n_0(t) = \int_0^t (\dot{\omega}_{H_2} + \dot{\omega}_{CO}) dt \quad (13)$$

where  $\Delta\delta(t)$  is the oxygen vacancy at each condition.  $n_0(t)$  and  $n_{LSCF}$  are the molar amount of total production (mol) and molar of the LSCF oxygen storage vacancy (mol).  $\dot{\omega}_{H_2}$  and  $\dot{\omega}_{CO}$  are the molar amount of  $\text{H}_2$  (mol) and molar amount of CO (mol).

The  $\Delta\delta$  of each condition, gathered in Table 1, is tabulated in Table 2 below:

**Table 2.** The spent oxygen vacancy at different conditions (refer to Table 1).

Condition No.	$\Delta\delta$
1	0.04
2	0.20
3	0.25
4	0.13
5	0.17
6	0.03
7	0.20
8	0.43
9	0.29
10	0.22
11	0.20

The maximum oxygen storage capacity was found under condition 8, where both the reduction and oxidation temperature were  $900\text{ }^\circ\text{C}$ , and the ratio of  $\text{H}_2\text{O}$  to  $\text{CO}_2$  was 3 to 1. It was noticeable that the poorest values of oxygen storage capacity (ranging from 0.03 to 0.13) were obtained if one of the reduction temperature or oxidation temperature was  $500\text{ }^\circ\text{C}$ . This was due to its low oxygen vacancy during the reduction step and/or its kinetic limitation during the oxidation step. All the oxygen storage capacities that were higher than 0.20 were obtained when the LSCF3773 was reduced at  $900\text{ }^\circ\text{C}$ . While the reduction temperature had a direct effect on the available oxygen storage capacity, the oxidation temperature seemed to influence the oxygen exchange capability.

### 3.5. Efficiency of the Dual Reactor System under 10 h Operation

The dual reactor was operated simultaneously, aiming to produce a continuous stream of products by switching between the reduction mode and oxidation mode. Both reactors were set as isothermal thermochemical cycles, meaning that both reduction and oxidation reactions were carried out at the same temperature,  $900\text{ }^\circ\text{C}$ , to reduce the time required for the temperature swing, thus increasing the overall efficiency of the process. Figure 8 illustrates the reduction and oxidation processes in which both the reduction/oxidation process each lasted for 15 min for each reactor before switching to another condition. During the 10 h experiment, 20 cycles of products were produced as shown below.

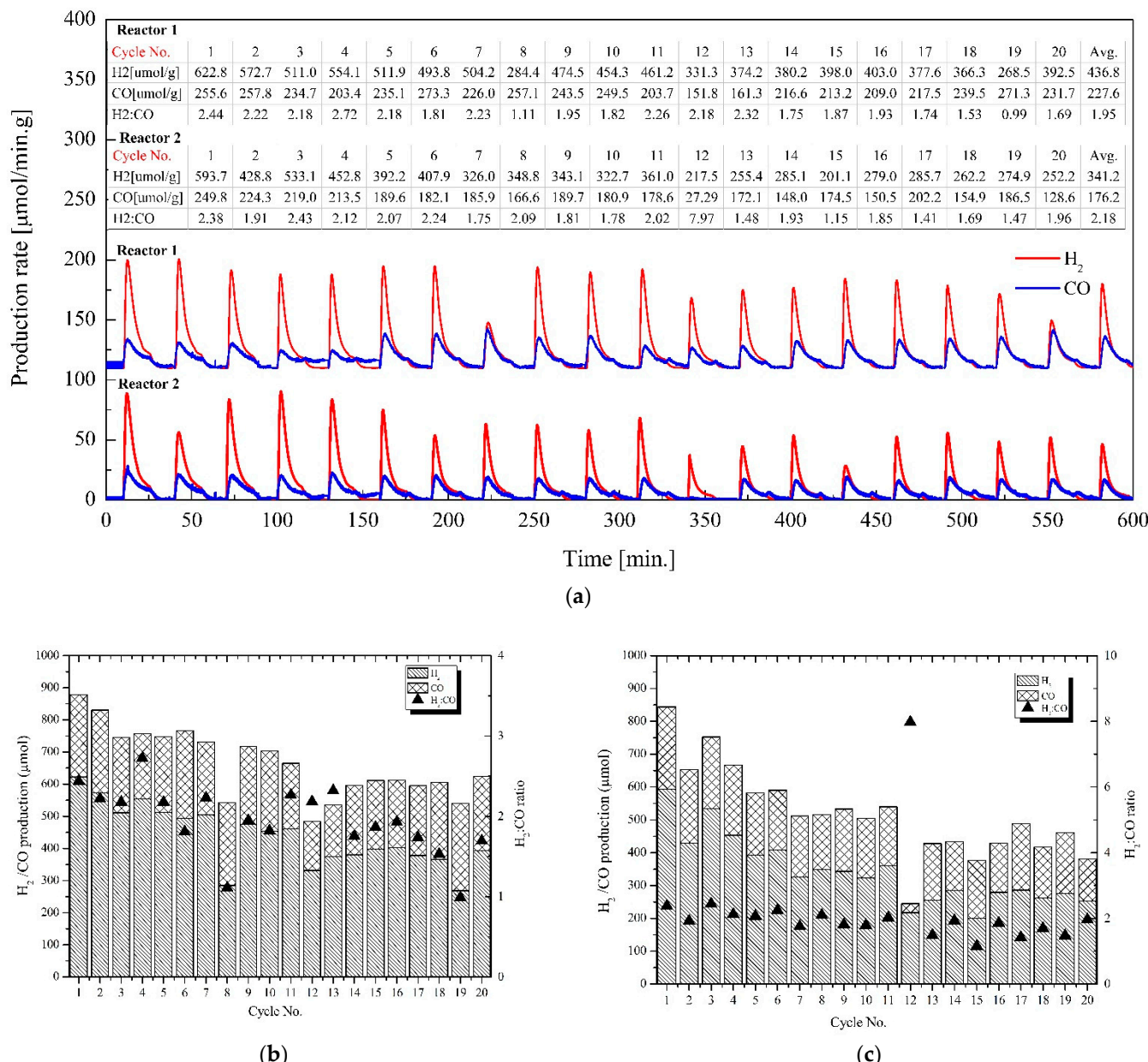


**Figure 8.** Productivities of  $\text{H}_2$  and  $\text{CO}$  in the dual-reactors system (a), total gas production and  $\text{H}_2:\text{CO}$  ratio of  $\text{H}_2\text{O}/\text{CO}_2$  co-splitting over LSFC3773 ( $T_{\text{red}}/T_{\text{ox}}$  were at  $900/900$   $^{\circ}\text{C}$ , feed ratio of  $\text{H}_2\text{O}$  to  $\text{CO}_2$  were 1 to 2.5) for 20 cycles from (b) reactor 1 and (c) reactor 2.

The productivity of both  $\text{H}_2$  and  $\text{CO}$  in both reactors were fluctuated; however, they tended to decrease by the increasing cycles, due to the loss of active sites caused by the  $\text{CO}_2$  blockage as described earlier. The overall production between the two reactors together was calculated at  $23,639.70 \mu\text{mol/g}$ . Similar experiments were carried out when the reduction and oxidation times were set at (1) reduction 30 min, oxidation 60 min, and (2) reduction 30 min, oxidation 30 min. The results are shown in Table 3.

From Table 3, it can be seen that the intervals of the reduction time of 30 min and oxidation time of 30 min showed the highest performance amongst all conditions, with the productivity of  $\text{H}_2$  and  $\text{CO}$  together at  $28,000 \mu\text{mol/g}$ . This isothermal thermochemical cycle was believed to be more effective than operating the reduction and oxidation processes optimally, i.e., running the experiment at the optimal reduction temperature at  $1200$   $^{\circ}\text{C}$  and oxidation temperature at  $900$   $^{\circ}\text{C}$  because the process loses time to pursue the

temperature swing (up to 90 min each cycle), resulting in a decrease in total productivity. Using only one operating temperature can reduce the thermal stress within the system. However, there is a chance that the reduction and oxidation can co-occur at the same time, which, in the worst case, might lead to an unwanted explosive mixture of H<sub>2</sub> and O<sub>2</sub>.

**Table 3.** Total productivity within 10 h at different reduction and oxidation time intervals.

Condition No.	Reduction Time (min)	Oxidation Time (min)	Number of Cycles in 10 h	Productivities ( $\mu\text{mol/g}$ )
1	15	15	20	23,640
2	30	60	7	25,200
3	30	30	10	28,000

### 3.6. Kinetic Study

The experimental data were compared to the simulated dataset derived from the kinetic model, using the non-linear regression method as described earlier in the methodology section. A target function ( $f$ ) was used to simulate the values with experimental data by varying the rate constant ( $k$ ). The initial reaction-controlled regime was chosen to calculate the kinetics parameters of H<sub>2</sub>O and CO<sub>2</sub> splitting. The reduction temperature was fixed at 900 °C for all cases, whereas the oxidation temperature was varied at 500, 700, and 900 °C, as shown in Figure 9.

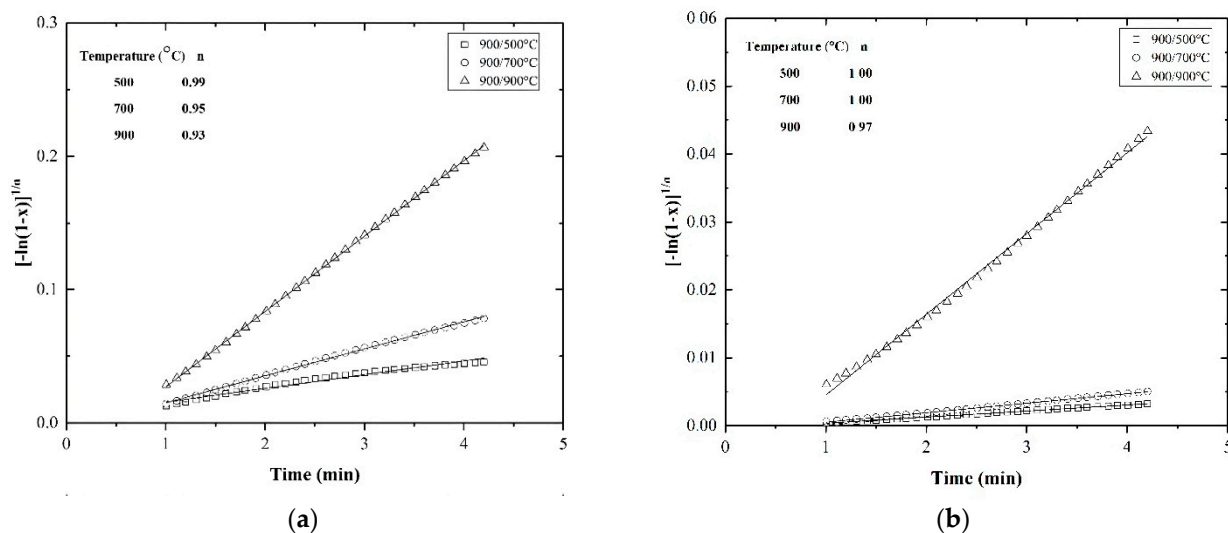


**Figure 9.** Plots of nucleation model, Avrami type vs. time toward H<sub>2</sub>O splitting (a), and CO<sub>2</sub> splitting (b) over LSCF3773 where the T<sub>red</sub> was fixed at 900 °C and T<sub>ox</sub> was varied at 500 °C (□), 700 °C (○) and 900 °C (△).

Figure 10 demonstrates the Arrhenius plots. The activation energy ( $E_a$ ) was represented as a linear function, as shown in Equations (14) and (15).

$$\ln k(T) = -3.7303 \left( \frac{1000}{T} \right) + 0.1911 \quad (14)$$

$$\ln k(T) = -5.7789 \left( \frac{1000}{T} \right) + 0.3047 \quad (15)$$

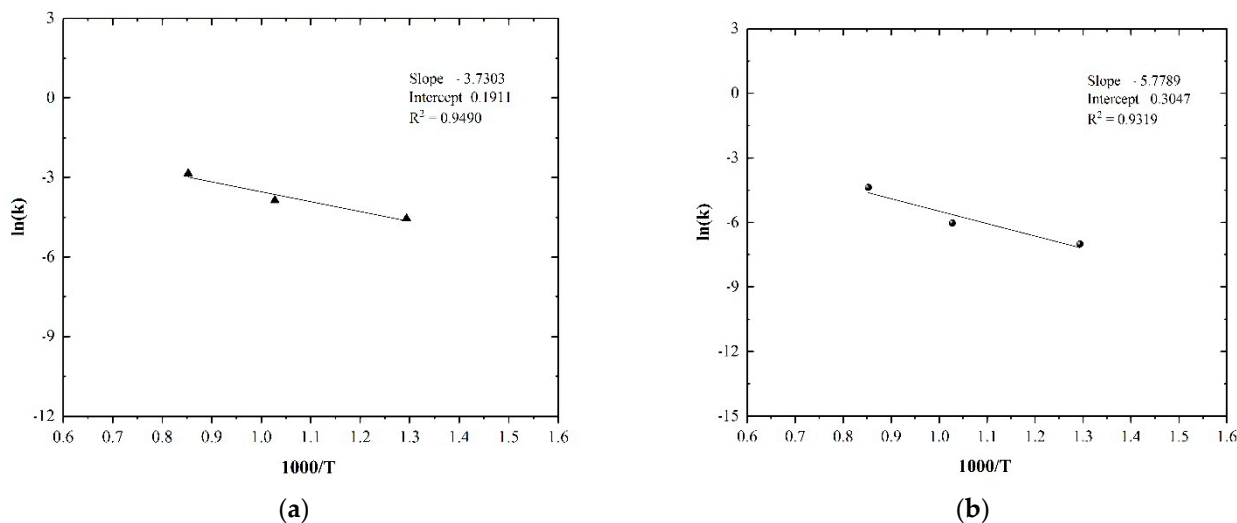


**Figure 10.** Logarithm of Arrhenius plot as a function of  $1000/T$  for  $\text{H}_2\text{O}$  splitting (a), and  $\text{CO}_2$  splitting (b) over LSCF3773.

The activation energy of  $\text{H}_2\text{O}$  and  $\text{CO}_2$  splitting over LSCF3773 was estimated at 31.01 and 48.05 kJ/mol, respectively.

#### 4. Conclusions

This work investigated the synthesis of gas production via thermochemical cycles co-feeding  $\text{H}_2\text{O}/\text{CO}_2$  using LSCF3773, which was synthesized using the EDTA-citrate complexing method. The oxygen storage capacity (OSC) was found to depend on the reduction temperature rather than the oxidation temperature. The highest  $\Delta\delta$  was achieved when the reduction and oxidation temperature were both fixed at 900 °C with the feed ratio ( $\text{H}_2\text{O}$  to  $\text{CO}_2$ ) of 3 to 1. With the increasing amount of  $\text{CO}_2$  in the feed mixture, CO productivity reached its plateau at high ratios of  $\text{H}_2\text{O}$  to  $\text{CO}_2$  (1:1, 1:2, and 1:2.5), while the total productivities were reduced during the same ratios. This indicated the existence of a  $\text{CO}_2$  blockage, which was the result of either high  $E_a$  of  $\text{CO}_2$  dissociation or high  $E_a$  of CO desorption, resulting in the loss of active species. From the results, it can be concluded that  $\text{H}_2\text{O}$  and  $\text{CO}_2$  splitting reactions are competitive reactions.  $E_a$  of  $\text{H}_2\text{O}$  and  $\text{CO}_2$  splitting was estimated at 31.01 kJ/mol and 48.05 kJ/mol, respectively, which agreed with the results obtained from the experimentation of the effect of the oxidation temperature. A dual reactor system was applied to provide a continuous product stream, for which the operation mode was switched between the reduction and oxidation step. The isothermal thermochemical cycle process, in which reduction and oxidation were performed at the same temperature, was also carried out in order to increase the overall efficiency of the process. The optimal time for the reduction and oxidation step was found to be 30 min each step with total productivity of the syngas mixture at 28,000  $\mu\text{mol/g}$ , approximately. Due to its excessive energy requirement for the reduction reaction, future work could consider combining a low temperature photo-catalytic chemical reaction for the reduction step, while the oxidation step could be carried out under a thermochemical reaction.

**Supplementary Materials:** The following are available online at <https://www.mdpi.com/article/10.3390/pr9061018/s1>.

**Author Contributions:** Conceptualization, U.W.H., T.S. and N.S.-N.; methodology, N.L.; software, T.K.; validation, U.W.H. and N.L.; formal analysis, T.K.; investigation, T.K., T.S., N.S.-N., U.W.H.; resources, T.S., N.S.-N.; data curation, N.L.; writing—original draft preparation, T.K.; writing—review and editing, U.W.H.; visualization, U.W.H.; supervision, U.W.H.; project administration, U.W.H.; funding acquisition, U.W.H. All authors have read and agreed to the published version of the manuscript.

**Funding:** This research is funded by Thailand Research Fund (RSA6180061 and PHD5910083), King Mongkut's University of Technology North Bangkok (KMUTNB-BasicR-64-31, KMUTNB-BasicR-64-34 and KMUTNB-PHD-62-10) and PTT Public company limited.

**Institutional Review Board Statement:** Not applicable.

**Informed Consent Statement:** Not applicable.

**Data Availability Statement:** Not applicable.

**Acknowledgments:** This work was supported by the Thailand Research Fund (RSA6180061 and PHD5910083), King Mongkut's University of Technology North Bangkok (KMUTNB-BasicR-64-31, KMUTNB-BasicR-64-34 and KMUTNB-PHD-62-10) and PTT Public company limited.

**Conflicts of Interest:** The authors declare no conflict of interest.

## References

1. Song, C.S. Global challenges and strategies for control, conversion and utilization of CO<sub>2</sub> for sustainable development involving energy, catalysis, adsorption and chemical processing. *Catal. Today* **2006**, *115*, 2–32. [[CrossRef](#)]
2. Olah, G.A.; Prakash Surya, G.K.; Goeppert, A. Anthropogenic chemical carbon cycle for a sustainable future. *J. Am. Chem. Soc.* **2011**, *133*, 12881–12898. [[CrossRef](#)]
3. Fletcher, E.A. Solarthermal processing: A review. *J. Sol. Energ. Eng.* **2001**, *123*, 63–74. [[CrossRef](#)]
4. Chueh, W.C.; Falter, C.; Abbott, M.; Scipio, D.; Furley, P.; Haile, S.M.; Steinfeld, A. High-flux solar-driven thermochemical dissociation of CO<sub>2</sub> and H<sub>2</sub>O using nonstoichiometric ceria. *Science* **2010**, *330*, 1797–1801. [[CrossRef](#)]
5. Le, G.A.; Abanades, S.; Flamant, G. CO<sub>2</sub> and H<sub>2</sub>O splitting for thermochemical production of solar fuels using nonstoichiometric ceria and ceria/zirconia solid solutions. *Energy Fuels* **2011**, *25*, 4836–4845.
6. Chueh, W.C.; Haile, S.M. A thermochemical study of ceria: Exploiting an old material for new modes of energy conversion and CO<sub>2</sub> mitigation. *Philos. Trans. R Soc. Lond. Ser. A* **2010**, *368*, 3269–3294. [[CrossRef](#)] [[PubMed](#)]
7. Abanades, S.; Chambon, M. CO<sub>2</sub> dissociation and upgrading from two-step solar thermochemical processes based on ZnO/Zn and SnO<sub>2</sub>/SnO redox pairs. *Energy Fuels* **2010**, *24*, 6667–6674. [[CrossRef](#)]
8. Gálvez, M.E.; Loutzenhiser, P.G.; Hischier, I.; Steinfeld, A. CO<sub>2</sub> splitting via two-step solar thermochemical cycles with Zn/ZnO and FeO/Fe<sub>3</sub>O<sub>4</sub> redox reactions: Thermodynamic analysis. *Energy Fuels* **2008**, *22*, 3544–3550. [[CrossRef](#)]
9. Loutzenhiser, P.G.; Gálvez, M.E.; Hischier, I.; Stamatiou, A.; Frei, A.; Steinfeld, A. CO<sub>2</sub> splitting via two-step solar thermochemical cycles with Zn/ZnO and FeO/Fe<sub>3</sub>O<sub>4</sub> redox reactions II: Kinetic analysis. *Energy Fuels* **2009**, *23*, 2832–2839. [[CrossRef](#)]
10. Venstrom, L.J.; Davidson, J.H. Splitting water and carbon dioxide via the heterogeneous oxidation of zinc vapor: Thermodynamic considerations. *ASME Conf. Proc.* **2010**, *2010*, 79–88.
11. Stamatiou, A.; Loutzenhiser, P.G.; Steinfeld, A. Syngas production from H<sub>2</sub>O and CO<sub>2</sub> over Zn particles in a packed-bed reactor. *AIChE J.* **2012**, *58*, 625–631. [[CrossRef](#)]
12. Loutzenhiser, P.G.; Elena, G.M.; Hischier, I.; Graf, A.; Steinfeld, A. CO<sub>2</sub> splitting in an aerosol flow reactor via the two-step Zn/ZnO solar thermochemical cycle. *Chem. Eng. Sci.* **2010**, *65*, 1855–1864. [[CrossRef](#)]
13. Loutzenhiser, P.G.; Meier, A.; Steinfeld, A. Review of the two-step H<sub>2</sub>O/CO<sub>2</sub>-splitting solar thermochemical cycle based on Zn/ZnO redox reactions. *Materials* **2010**, *3*, 4922–4938. [[CrossRef](#)]
14. Stamatiou, A.; Loutzenhiser, P.G.; Steinfeld, A. Solar syngas production via H<sub>2</sub>O/CO<sub>2</sub>-splitting thermochemical cycles with Zn/ZnO and FeO/Fe<sub>3</sub>O<sub>4</sub> redox reactions. *Chem. Mater.* **2009**, *22*, 851–859. [[CrossRef](#)]
15. Khamhangdatepon, T.; Tongnan, V.; Hartley, M.; Sornchamni, T.; Siri-Nguan, N.; Laosiripojana, N.; Li, K.; Hartley, U.W. Mechanisms of synthesis gas production via thermochemical cycles over La<sub>0.3</sub>Sr<sub>0.7</sub>Co<sub>0.7</sub>Fe<sub>0.3</sub>O<sub>3</sub>. *Int. J. Hydrogen Energy* **2020**. [[CrossRef](#)]
16. Nair, M.M.; Abanades, S. Experimental screening of perovskite oxides as efficient redox materials for solar thermochemical CO<sub>2</sub> conversion. *Sustain. Energy Fuels* **2018**, *2*, 843–854. [[CrossRef](#)]
17. Wang, L.; Al-Mamun, M.; Liu, P.; Wang, Y.; Yang, H.G.; Zhao, H. Notable hydrogen production on La<sub>x</sub>Ca<sub>1-x</sub>CoO<sub>3</sub> perovskites via two-step thermochemical water splitting. *J. Mater. Sci.* **2018**, *53*, 6796–6806. [[CrossRef](#)]
18. Orfila, M.; Linares, M.; Molina, R.; Botas, J.Á.; Sanz, R.; Marugán, J. Perovskite materials for hydrogen production by thermochemical water splitting. *Int. J. Hydrot. Energy* **2016**, *41*, 19329–19338. [[CrossRef](#)]
19. Wang, L.; Al-Mamun, M.; Zhong, Y.L.; Liu, P.; Wang, Y.; Yang, H.G.; Zhao, H. Enhanced thermochemical water splitting through formation of oxygen vacancy in La<sub>0.6</sub>Sr<sub>0.4</sub>BO<sub>3-δ</sub> (B = Cr, Mn, Fe, Co, and Ni) Perovskites. *ChemPlusChem* **2018**, *83*, 924–928. [[CrossRef](#)]
20. Bork, A.H.; Kubicek, M.; Struzik, M.; Rupp, J.L.M. Perovskite La<sub>0.6</sub>Sr<sub>0.4</sub>Cr<sub>1-x</sub>Co<sub>x</sub>O<sub>3-δ</sub> solid solutions for solar-thermochemical fuel production: Strategies to lower the operation temperature. *J. Mater. Chem. A* **2015**, *3*, 15546–15557. [[CrossRef](#)]
21. Demont, A.; Abanades, S.; Beche, E. Investigation of perovskite structures as oxygen-exchange redox materials for hydrogen production from thermochemical two-step water-splitting cycles. *J. Phys. Chem. C* **2014**, *118*, 12682–12692. [[CrossRef](#)]

22. Sibieude, F.; Ducarroir, M.; Tofighi, A.; Ambriz, J. High temperature experiments with a solar furnace: The decomposition of  $\text{Fe}_3\text{O}_4$ ,  $\text{Mn}_3\text{O}_4$ ,  $\text{CdO}$ . *Int. J. Hydrogen Energy* **1982**, *7*, 79–88. [[CrossRef](#)]
23. Charvin, P.; Abanades, S.; Flamant, G.; Lemort, F. Two-step water splitting thermochemical cycle based on iron oxide redox pair for solar hydrogen production. *Energy* **2007**, *32*, 1124–1133. [[CrossRef](#)]
24. Ding, X.; Liu, Y.; Gao, L.; Guo, L. Synthesis and characterization of doped  $\text{LaCrO}_3$  perovskite prepared by EDTA–citrate complexing method. *J. Alloy. Compd.* **2008**, *458*, 346–350. [[CrossRef](#)]